Research Article

Smart Pillow Based on Flexible and Breathable Triboelectric Nanogenerator Arrays for Head Movement Monitoring during Sleep

Haiying Kou,[⊥] Haiming Wang,[⊥] Renwei Cheng,[⊥] Yanjun Liao, Xue Shi, Jianjun Luo, Ding Li,* and Zhong Lin Wang*

Cite This: https://doi.org/10.1021/acsami.2c03056

Read Online

ACCESS | 📊 Metrics & More | 📖 Article Recommendations | 🆘 Supporting Information

ABSTRACT: Sleep quality plays an essential role in human health and has become an index for assessing physical health. Self-powered, sensitive, noninvasive, comfortable, and low-cost sleep monitoring sensors for monitoring sleep behavior are still in high demand. Here, a pressure-sensitive, noninvasive, and comfortable smart pillow is developed based on a flexible and breathable triboelectric nanogenerator (FB-TENG) sensor array, which can monitor head movement in real time during sleep. The FB-TENG is based on flexible and breathable porous poly(dimethylsiloxane) (PDMS) with a fluorinated ethylene propylene (FEP) powder and exhibits pressure sensitivity and durability. The electrical output of the FB-TENG is further optimized by modifying the porous structure and the FEP powder. Combining the FB-TENG and the flexible printed circuit (FPC), a self-powered pressure sensor array is fabricated to realize touch sensing and motion track monitoring. The smart pillow is formed by laying the self-powered pressure sensor array on an ordinary pillow to realize real-time monitoring of the head position in a static state and head movement trajectory in a dynamic state during sleep. Additionally, the smart pillow also has an early warning function for falling out of bed. This work not only provides a viable sensing device for sleep monitoring but also could be extended to real-time monitoring of some diseases, such as brain diseases and cervical spondylosis, in the future. It is expected to introduce a practical strategy in the real-time mobile healthcare field for disease management.

KEYWORDS: sleep monitoring, smart pillow, triboelectric nanogenerator, pressure sensor array, head movement
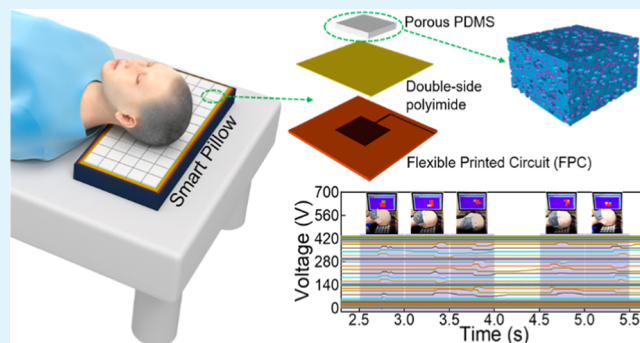
1. INTRODUCTION

Nowadays, with the improvement of human living standards and quality, people pay more and more attention to their health. At the same time, with the rapid development of science and technology, health monitoring products that can reflect physical health status have gradually entered the daily life with functions of blood pressure monitoring,[1,2] heart rate monitoring,[3,4] arterial pulse monitoring,[5,6] respiration monitoring,[7,8] etc. Sleep, as one of the natural physiological phenomena for human beings, is closely related to human health and can make the human brain and body recover from fatigue.[9] Poor sleep may lead to poor mood,[10] slow reflexes,[11] memory loss,[12] etc. Long-term poor sleep might cause coronary heart disease, hypertension, neurasthenia, and is life-threatening in severe cases.[13,14] Hence, real-time and continuous sleep monitoring is necessary for human health monitoring. At present, a traditional sleep monitoring product (such as polysomnography[15,16]) is limitedly used in hospitals for its high cost and complex structure. Smart phones[17,18] and smart watches[19,20] are commonly used for monitoring sleep in daily life. Compared to polysomnography, they are small and convenient but might be affected by poor wearing comfort, low

detection sensitivity, radiation, and external power supply. Therefore, it is imperative to develop a sleep monitoring product with a simple structure, low cost, self-powered supply, noninvasive usage, comfortable experience, and high sensitivity.

Triboelectric nanogenerators (TENGs)[21−25] are a new class of technology based on frictional electrification and electrostatic induction coupling, which can be used for energy harvesting,[26,27] high-voltage sources,[28] and a self-powered sensor.[29] Combining its simple structure, low cost, wide selection of materials, and self-powered features, many research works have been devoted to sleep monitoring based on a self-powered TENG sensor.[30−36] These sensors in the form of eye masks,[30] patches,[31−33] or belts[34] could analyze sleep behavior by monitoring eyes, limbs, or breath movements. However,

users need to wear these sensors and might not fall asleep in their most natural ways. Meanwhile, the wearing of a belt and an eye mask might bring a sense of restraint and cause sleep discomfort. In addition, the impermeability of patches may cause discomfort to human skin. To address these issues, the smart textile-based TENG is proposed as a noninvasive bed sheet to monitor sleeping by monitoring the sleeping posture.[35,36] Probably, it is the lack of comfortable materials and low sensing resolution (normally at a level of 10×10 cm^2 for one sensor), which is not enough for precise head monitoring. Most of the current research studies on sleep monitoring do not consider head movement when monitoring the sleeping posture. However, the head is a key part of the body, which directly protects and affects the brain. It is ideal to analyze its behavior during sleep with comfortable materials and higher sensing resolution.

In this work, a pressure-sensitive, noninvasive, breathable, and comfortable smart pillow is developed based on a flexible and breathable triboelectric nanogenerator (FB-TENG) pressure sensor array for the head movement monitoring and the falling out of bed alarm function. The FB-TENG is assembled based on porous poly(dimethylsiloxane) (PDMS) containing a fluorinated ethylene propylene (FEP) powder produced by the sacrificial template method.[37−39] The electrical output of FB-TENG is improved by adjusting the content of the FEP powder and the size of the pores. The final FB-TENG is featured with flexibility, air permeability, excellent stability, and high sensitivity. Taking the flexible printed circuit (FPC) containing the copper electrode array as a working electrode, a self-powered pressure sensor array is fabricated with 8×8 FB-TENGs to realize tactile sensing and motion track monitoring at the same time. Furthermore, a smart pillow, formed by placing this pressure sensor in a 5×12 array on an ordinary pillow, can record real-time head movement during sleep and provide early warning of emergencies. This sensitive, noninvasive, breathable, and comfortable smart pillow provides a new strategy for sleep monitoring, which may have broad applications in the fields of the personal healthcare system.

2. RESULTS AND DISCUSSION

The porous PDMS is chosen to achieve the flexibility and air permeability of a smart pillow based on FB-TENG. The fabrication process is depicted in Scheme 1. Citric acid monohydrate (CAM) particles and FEP powder were added to the PDMS mixed solution. After stirring and curing, the mixture was immersed in ethanol to dissolve CAM. Eventually, a porous structure was formed for further assembly into the FB-TENG (Scheme S1). The detailed fabrication process is described in the Experimental Section. Figure S1 shows the

Scheme 1. Schematic Diagram of the Fabrication Process of the Porous PDMS and the FB-TENG in a Single-Electrode Mode

• FEP   • CAM   ▬ Kapton   ▬ Al electrode   ▢ Acrylic
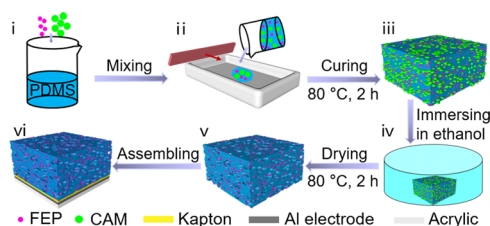
morphology and the size distribution of three kinds of CAM particles at 860 ± 70, 290 ± 16, and 74 ± 6 μm. Porous PDMS can be formed by sacrificing CAM particles. Figure S2a illustrates the physical image of the prepared porous PDMS using 74 ± 6 μm CAM particles and 10 wt % FEP powder. It can be easily stretched, bent, and twisted by hands (Figure 1a),
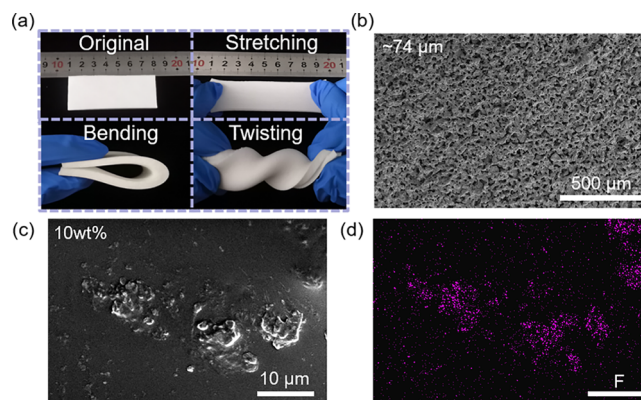

Figure 1. Basic characteristics of porous PDMS (made with 74 ± 6 μm CAM particles and 10 wt % FEP powder). (a) Mechanical characteristics of porous PDMS of stretching, bending, and twisting; (b) SEM image of the porous PDMS; and (c, d) SEM image and EDS image of the PDMS with an FEP content of 10 wt %.

which exhibits excellent mechanical flexibility. Its mechanical strength is shown in Figure S2b, and a weight of 1 kg can be suspended by it without breaking. It is also resilient; the porous structure ensures that it can maintain 99.9% of its initial height after being compressed by 50% (Figure S2c). The air permeability of a porous PDMS film increases by 7−8 magnitude compared with that of the solid PDMS film, which has almost no air permeability under the same air pressure (Figure 3d). These excellent features mainly originated from the porous structure. The porous structure of PDMS fabricated from 74 ± 6 μm CAM particles is magnified in the scanning electron microscopy (SEM) image (Figures 1b and S3), where the pores size corresponds to the CAM particles (Figure S1c). The saddle-backings on the PDMS (10 wt % FEP powder) surface are the accumulation of the FEP powder, which could be distinguished by F (from FEP) element and Si (from PDMS) element distributions through the SEM image and the corresponding energy-dispersive spectrometry (EDS) diagrams shown in Figures 1c,d and S4. Thus, the porous PDMS (made with 74 ± 6 μm CAM particles and 10 wt % FEP powder) with flexibility, resilience, and air permeability is assembled into FB-TENG and spread on ordinary pillows to monitor head movement.

The basic working mechanism of the FB-TENG based on the flexible and breathable porous PDMS can be explained as a coupling between triboelectrification and electrostatic induction. Under the action of cycled external force, the schematic diagram of the working principle of the FB-TENG is shown in Scheme 2. After the Al electrode is connected to the ground through a metal wire, the FB-TENG will work in a single-electrode mode that makes the FB-TENG suitable as a pressure sensor to monitor the head movement. The single-sided polyimide tape (Kapton film), which is chosen to represent the parts of the head such as skin and hair for illustrating purposes, is used as a movable friction material driven by a linear motor. In the initial state, the Kapton film

Scheme 2. Working Mechanism of the FB-TENG in a Single-Electrode Mode
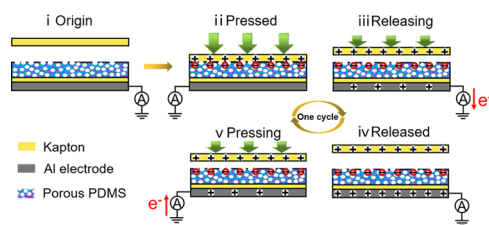
and the porous PDMS are not in contact, so there is no charge transfer (Scheme 2i). Once contact and friction between two materials occurred by the external force, the electrons are transferred from the Kapton film to the porous PDMS due to their different abilities to acquire electrons. It results in the same amount of positive and negative charges generated on both materials (Scheme 2ii). When two materials are separated, the positive charges are induced on the Al electrode to balance the negative charges on the porous PDMS, thus the electrons are transferred from the ground to the Al electrode through an external circuit (Scheme 2iii), generating a negative current signal (Figure S5). Until the external force is completely removed, the same amount of charges is induced on the Al electrode as those on the porous PDMS (Scheme 2iv). When the Kapton film and the porous PDMS are close to each other again by the external force, the reverse situation of the electrons transfer occurs (Scheme 2v and generates a positive current signal (Figure S5). Hence, when the external force is applied cyclically, the FB-TENG works cyclically according to this working principle.

Based on this working principle, a series of basic electrical output performances of the FB-TENG (2×2 cm^2) with a 10

wt % FEP powder content in porous PDMS (made with 74 ± 6 μm CAM particles) were tested. The open-circuit voltage (V_{oc}), the short-circuit current (I_{sc}), and the short-circuit transferred charge (Q_{sc}) under different frequencies (0.5−3.0 Hz) are shown in Figures 2a and S6. There is almost no change in the V_{oc} and Q_{sc} at different frequencies, but the I_{sc} increases as the frequency increases. Figure S7a shows the output power of the FB-TENG and the current of the external circuit when the applied external force is 20 N and the external load resistance changes from 1 to 9 GΩ. As the external load resistance increases, the current of the external circuit reduces. The output power reaches the maximum at an external load resistance of 6 GΩ. Movie S1 (Supporting Information) demonstrates that the FB-TENG (2×2 cm^2) could light up 14 LEDs under the drive of a linear motor with an external force of 20 N at a frequency of 1.0 Hz. Figure S7b exhibits the charging curve of the FB-TENG charging different capacitors from 0 to 2.5 V under a frequency of 3.0 Hz and an external force of 20 N, indicating that the charging rate increases as the capacitance decreases. It only takes about 0.8 s to charge the 0.22 F capacitor to 2.5 V. To highlight the durability of the FB-TENG, the V_{oc} of the FB-TENG is tested with a frequency of 3.0 Hz under an external force of 20 N for about 14,000 cycles and it does not have any significant reduction (Figure 2b). Considering that the pressure sensitivity is a key factor, the FB-TENG should be sensitive to external force. The real-time V_{oc}, I_{sc}, and Q_{sc} under different external forces are demonstrated in Figures 2c and S8. It can be clearly seen that the value of the V_{oc}, I_{sc}, and Q_{sc} increases as the pressure increases, which can be explained by the fact that the electrical output increases with the large effective contact area caused by the large pressure.[40] The pressure sensitivity of the FB-TENG under different pressures is shown in Figure 2d. It can be divided into
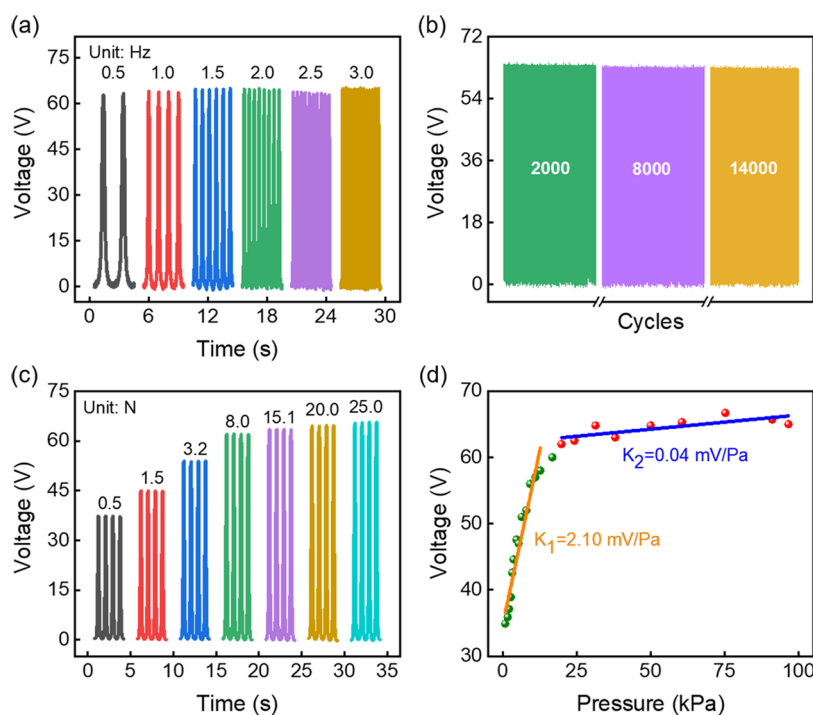

Figure 2. Basic electrical output performance of the FB-TENG (made with 74 ± 6 μm CAM particles and 10 wt % FEP powder) in a single-electrode mode. (a) V_{oc} of the FB-TENG at various applied frequencies (0.5−3.0 Hz), (b) V_{oc} under more than 10,000 cycles, (c) real-time output voltage under different forces, and (d) sensitivity curve under different pressures.
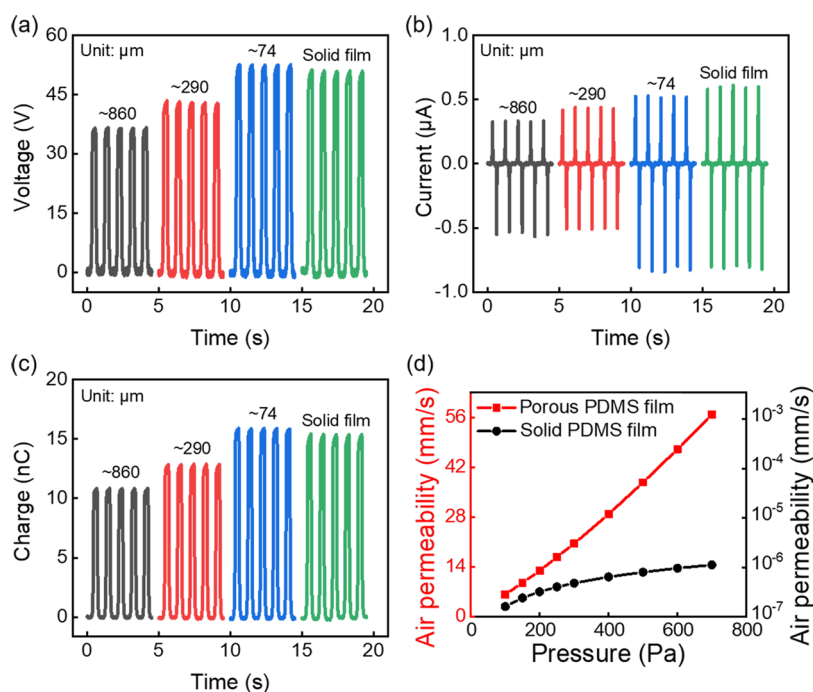
Figure 3. Influence of the size of CAM particles on the electrical output of the FB-TENG. (a) V_{oc}, (b) I_{sc}, and (c) Q_{sc} of the FB-TENG at a size of 860 ± 70, 290 ± 16, and 74 ± 6 μm CAM particles without FEP and a solid PDMS film under an external force of 20 N. (d) Air permeability of the porous PDMS film (made with 74 ± 6 μm CAM particles and 10 wt % FEP powder) and the solid PDMS film.

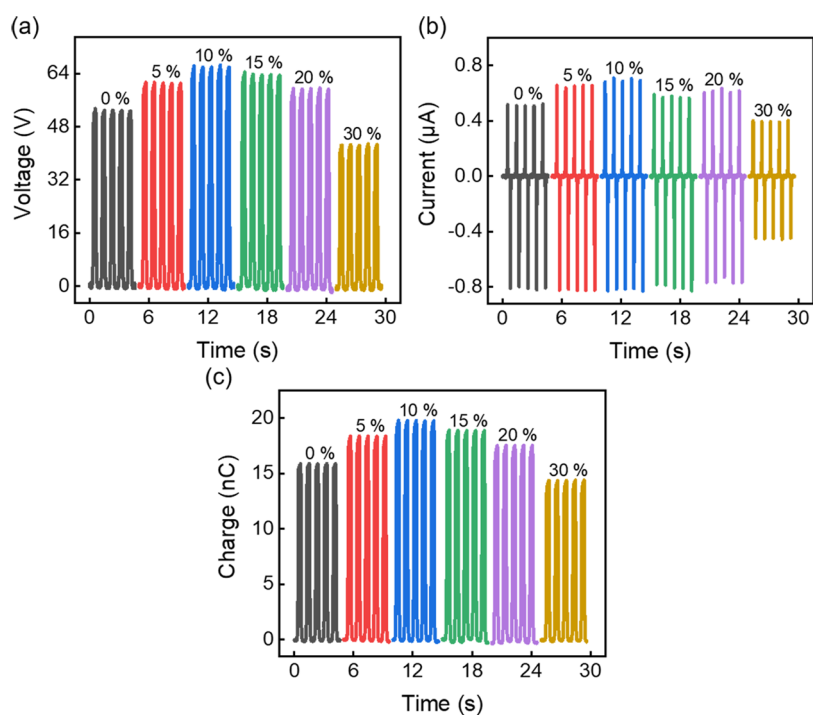**Figure 4.** Influence of the content of FEP powder on the electrical output of the FB-TENG. (a) V_{oc}, (b) I_{sc}, and (c) Q_{sc} of the FB-TENG at a size of 74 ± 6 μm CAM particles with the FEP powder content ranging from 0 to 30 wt % under an external force of 20 N.

two regions. The first region is the low-pressure region (<15 kPa) with a pressure sensitivity of 2.10 mV Pa^{-1}; the second region is the high-pressure region (>15 kPa) with a pressure sensitivity of 0.04 mV Pa^{-1}. The voltage in the low-pressure region has a better response to the increase in pressure than in the high-pressure region, which can be attributed to the increase in the effective contact area in the low-pressure region. Moreover, considering that the weight of the human head is

around 5 kg, the average pressure over 10 FB-TENGs (each one is 2 × 2 cm²) is about 12.5 kPa. Therefore, the normal pressure of a human head on our smart pillow during sleep just corresponds to our high sensitivity region (low-pressure region).

The effective contact area influences the electrical output of FB-TENG, and it is closely related to the size of the formed porous structure determined by the size of the selected CAM
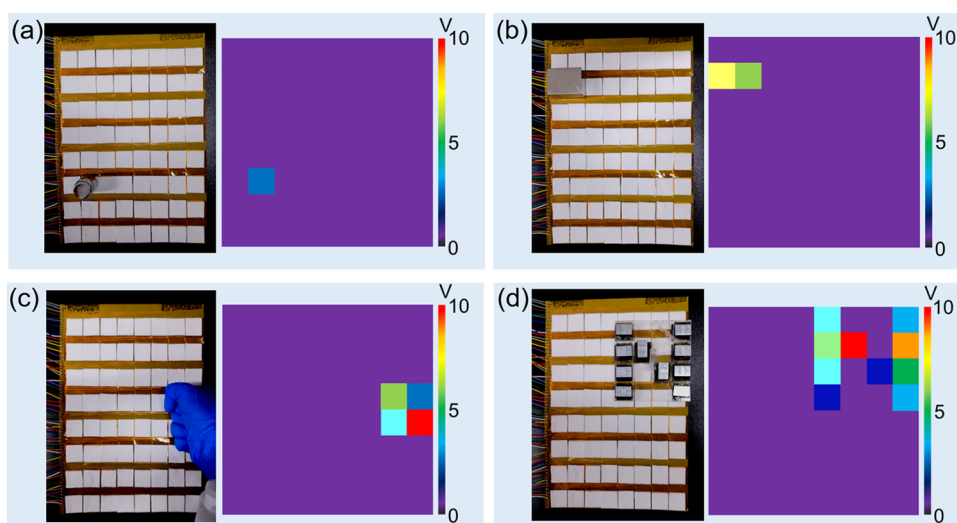
Figure 5. Application of the FB-TENG array in pattern mapping. (a−d) Demonstration and the two-dimensional output voltage intensity schematic diagram of a weight, a rectangular square, a fist, and an N-letter shape model.

particles. Therefore, we discuss the influence of the CAM particle size on the electrical output. The electrical outputs of FB-TENGs ($2.0 \times 2.0 \times 0.3$ cm^3) with CAM particles sizes of 860 ± 70, 290 ± 16, and 74 ± 6 μm were measured. In addition, these results were compared with the electrical output of the TENG composed of a solid PDMS film without porous structures. Figures 1b and S9a show the SEM image of the surface of porous PDMS and a solid PDMS film. The small-size CAM particles correspond to small-size pores, and no pore was observed on the surface of the solid PDMS film. The V_{oc}, I_{sc}, and Q_{sc} of the TENGs based on these four structures without FEP under an external force of 20 N are presented in Figure 3a−c, respectively. Compared with the FB-TENG made with 860 ± 70 μm CAM particles, the output of the one made with 74 ± 6 μm CAM particles increases by 1.5 times. This may be attributed to the larger effective contact area resulting from the smaller size of CAM particles. The increase in the effective contact area leads to more triboelectric charges, which will further increase the electrical output. Different from the previous literature,[41] where the electrical signals were generated from the contact separation between different materials inside the pores, our FB-TENG generates electrical signals from the charged surface of porous PDMS. The porous structure is served for the aim of a soft and breathable (Figure 3d) device to meet the needs of smart pillows, and the materials inside the pores are same. Compared with solid PDMS, porous PDMS with large pores gives a more comfortable experience and breathability but a lower electrical output due to the reduction of the effective contact area. The output of the FB-TENG increases with the decrease in pore size until the output of FB-TENG with a 74 ± 6 μm pore size is similar to that of a solid PDMS. Therefore, it is chosen for the following experiments of head monitoring.

Moreover, the FEP powder content also has an impact on the electrical output. Based on FB-TENG made with 74 ± 6 μm CAM particles, the V_{oc}, I_{sc}, and Q_{sc} of FB-TENG with the FEP powder content ranging from 0 to 30 wt % are shown in Figure 4a−c, respectively. When the content of the FEP powder increases in the range of 0−30 wt %, the V_{oc}, I_{sc}, and Q_{sc} of FB-TENG reach the maximum value when the FEP powder content is 10 wt %. More content of FEP powder does

not have a more positive effect, which might be attributed to the following reason. As shown in Figures 1c and S9b, the higher the content of the FEP powder (more than 10 wt %), the more clusters are gradually generated, which may modify the surface by covering the original surface. The triboelectric properties of the PDMS surface are affected, resulting in a decrease in the electrical output. Thus, the optimized content of the FEP powder is 10 wt %.

To demonstrate the practical usage of the FB-TENG as a self-powered pressure sensor, a flexible self-powered triboelectric sensor array was fabricated. The detailed fabrication process is shown in Figure S10a. An 8×8 copper array (the area of each one is 2×2 cm^2) was designed based on the FPC as a working electrode. Then a friction material, the prepared porous PDMS (made with 74 ± 6 μm CAM particles and 10 wt % FEP powder at the size of 2×2 cm^2), was glued together with the FPC containing the electrode array through double-sided polyimide tape. Eventually, an 8×8 FB-TENG sensor array with a three-layer structure was obtained. The completed flexible sensor array is shown in Figure S10b. It combines the sensing properties of the FB-TENG and the flexibility of the FPC. Each FB-TENG unit is connected to an independent channel, and the data are obtained by a multichannel data acquisition system (Figure S10c). For example, when a finger touches the surface of the sensor array, the FB-TENG at the corresponding position will generate a real-time output signal. The multichannel data acquisition system will receive the signals from the sensor array at the same time. Then, the multichannel signal statistics program will reflect the real-time data after the data processing. The specific information of the multichannel signal statistics program is embodied in Figure S11, including a signal distribution map, a signal frequency statistics chart, and a real-time voltage signal acquisition of an 8×8 array. To distinguish each unit, the FB-TENG sensor array is numbered in rows and columns, as shown in Figure S10a. For example, Ri−Cj represents the FB-TENG sensor unit located in the i-th row and the j-th column. The position, where the signal comes from, could be conveniently located by the numbered sensor array. When a 100 g weight and a rectangular square with a weight of 234 g are located at different positions of the sensor array, the physical image and
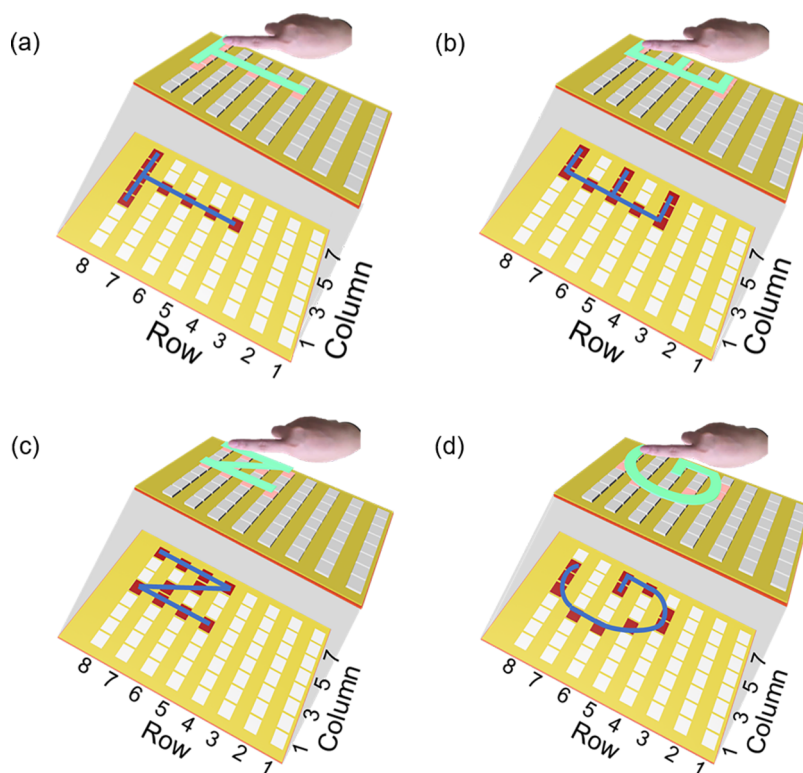
Figure 6. Application of the FB-TENG array in trajectory monitoring. (a−d) Schematic diagram of a finger writing letters T, E, N, and G on the surface of the 8 × 8 FB-TENG sensor array.
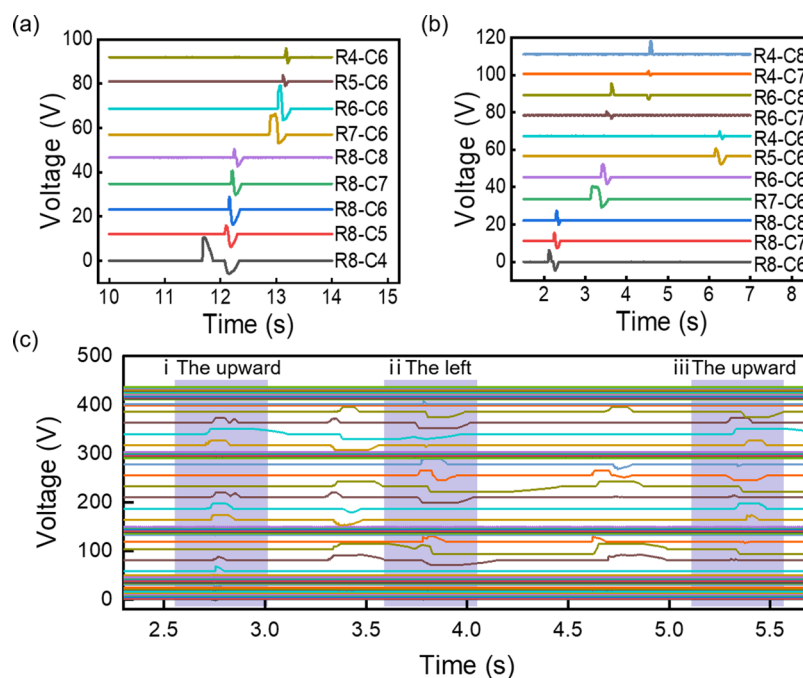

Figure 7. Output voltage signals for corresponding trace monitoring. (a, b) Real-time output voltage when writing T and E with a finger and (c) corresponding output signal during the head turning from the upward to the left and then back to the upward.

the corresponding two-dimensional output voltage intensity schematic diagram are shown in Figure 5a,b, respectively. The sensor array can respond sensitively to different pressures: the higher the pressure, the higher the corresponding output voltage appears. The physical image and the corresponding two-dimensional voltage intensity schematic diagram, when a fist and an N-letter shape model are located on the surface of

the sensor array, are shown in Figure 5c,d, respectively. The two-dimensional voltage intensity schematic diagram can reflect the real-time pressure distribution and map the specific pattern of the object. The corresponding three-dimensional (3D) real-time output voltages of the weight, rectangular square, fist, and N-letter shape model are displayed in Figures S12 and S13. The video of the single-point and multipoint

tactile sensing function of this sensor array is given in Movie S2 (Supporting Information). Furthermore, this sensor array can also be used to monitor the motion trajectory of moving objects. Figure 6a−d and Movie S3 (Supporting Information) demonstrate that a finger slides on the surface of the sensor array according to the trajectory of the letter "T", "E", "N", and "G", and the corresponding real-time output voltage is shown in Figures 7a,b, and S14. It shows that the output voltage signals of the corresponding units are recorded in the order of time, and the sliding track of the finger can be recognized. Therefore, the FB-TENG sensor array can realize simple graph mapping during multipoint contact and trajectory tracking when objects are in motion. The above results demonstrate that the sensor array composed of the FB-TENG has the potential to be applied to real-time tactile sensing and motion trajectory monitoring of external objects, such as head monitoring.

Postural change is an important parameter in sleep monitoring, which can be used as key information for evaluating sleep quality. Real-time head movements are important parts of postural change, which could also reflect changes in the state of the entire body during sleep. Combining the flexibility and breathability of porous PDMS and the application potential of FB-TENG pressure-sensing array in pressure distribution mapping (touch sensing) and motion trajectory monitoring, a smart pillow was developed for the monitoring of head movements, reflecting body turnover during sleep (Figure S15a). Figure S15b shows the physical image of the smart pillow, which is fabricated by simply laying the 5 × 12 FB-TENG pressure-sensing array fabricated by the same preparation method as shown in Figure S10a on the ordinary pillow. The same multichannel acquisition system as shown in Figure S10c is used to collect the output signal of the smart pillow. That is, when the head is on the smart pillow, the FB-TENG units in the corresponding position would be triggered to generate the output signals, and the signals would be captured by the multichannel acquisition card and then processed and reflected in the computer program interface. In the experimental demonstration, a head model was manually controlled to move on the smart pillow to simulate actual sleep movements. As shown in Figure S16a, when the head model is lying on the smart pillow, the corresponding two-dimensional voltage intensity map that can reflect the head pressure distribution is shown in Figure S16b, and the real-time 3D output voltage is shown in Figure S16c. In addition, a high spatial resolution of the contact pressure of the head is achieved through multiple pressure-sensing units as shown in these figures, which is at least 4 times higher than previous reports.[35,36] Figures 7c and 8a demonstrate the real-time information of head turning from the upward to the left and then back to the upward. The smart pillow could clearly record the movement of the head during this procedure with voltage changes in each channel and illustrate the pressure distribution of the head movement by the real-time two-dimensional voltage intensity map. More information on the head position, posture, and pressure distribution is given in Figure S17 and Movie 4 (Supporting Information). Under static conditions, the two-dimensional voltage intensity map can detect the presence and posture changes of the head on the smart pillow; under dynamic conditions, the two-dimensional voltage intensity map changes continuously when the head moves on the smart pillow caused by body turning, which can be used to identify postural changes during sleep. Therefore, by collecting
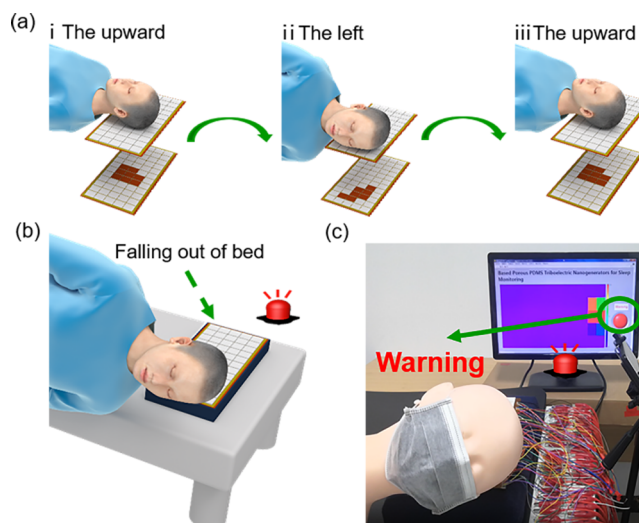

Figure 8. Application of the FB-TENG array as a smart pillow in monitoring head movement. (a) Demonstration diagram of the head turning from the upward to the left and then back to the upward. (b) Schematic diagram when a person is in danger of falling out of bed. (c) Demonstration diagram of triggering the alarm system when the head moves to the edge column.

the output voltage signal, not only the distribution of the head pressure can be clearly reflected but also the movement of the head can be recorded and detected at the same time, and then the body position change can be reflected accordingly. In practical applications, parents or doctors can analyze the sleep situation of children or patients through the recorded output signals.

Furthermore, a smart pillow could also be used to design an early warning system for falling out of bed. Babies and the elderly with poor self-care ability or unconscious patients might turn over and move to the edge of the bed unconsciously during sleep, which would be in danger of falling out of bed (Figure 8b). Therefore, we designed an early warning function based on the smart pillow to detect whether the head is moved to the most edge position of the smart pillow. If the five TENG pressure-sensing units located at the most edge position are touched by the head (Figure S18), the resulting output signal would trigger the alarm system, as demonstrated in Figure 8c and Movie 5 (Supporting Information). Thereby, it could remind the guardian or doctor to adjust their sleeping position and avoid the danger of falling out of bed. Moreover, this smart pillow could also be extended to real-time monitoring of some diseases, such as brain diseases and cervical spondylosis, in the future. This smart pillow is expected to open up a novel solution for real-time mobile disease management and bring convenience to patients.

3. CONCLUSIONS

In conclusion, we propose a smart pillow design for real-time monitoring of head movement during sleep. We fabricated a flexible, breathable, and stretchable porous PDMS containing FEP powder by the sacrificial template method. Based on this porous PDMS, we assembled a FB-TENG with good durability and pressure sensitivity. Based on the FB-TENG, an 8 × 8 sensor array was integrated. It not only realizes simple pattern mapping but also achieves the trajectory tracking of moving objects. Furthermore, a pressure-sensitive, flexible, and breath-able smart pillow was made by laying a 5 × 12 FB-TENG

pressure sensor array on an ordinary pillow for head movement monitoring. The smart pillow can recognize the movements of the head and record real-time head pressure distribution when turning over during sleep. Moreover, this smart pillow can realize a self-powered alarm to remind the guardian when people under guardianship are in danger of falling out of bed. Given the simplicity of equipment production, the smart pillow in this work can be designed and produced according to various actual conditions and let people sleep in their natural ways. This work is expected to provide another possibility for the field of human—machine interactive sleep behavior monitoring. Finally, we also expect that it could generate an important impact on self-powered motion tracking, intelligent tactile perception, remote health monitoring, and other fields.

4. EXPERIMENTAL SECTION

4.1. Fabrication of the Flexible and Breathable Porous PDMS. A sacrificial template technique[37−39] was used to fabricate the flexible and breathable porous PDMS. The fabrication process is shown in Scheme 1. Initially, a PDMS elastomer and a curing agent (Sylgard 184, Dow Corning) were evenly mixed in a weight ratio of 10:1, and a vacuum was applied to remove air bubbles. Then, a certain amount of CAM particles, with the sizes of 860 ± 70, 290 ± 16, and 74 ± 6 μm were, respectively, screened out by the sieves with apertures of 900 and 710, 300 and 250, and 74 and 65 μm, and different mass ratios (0, 5, 10, 15, 20, and 30 wt %) of FEP powder were sequentially added into the prepared PDMS mixture. After stirring evenly, the mixture was transferred into a prepared mold of a certain size (5×7 cm^2), and then it was placed in an oven at 80 °C for 2 h curing. Next, the cured sample was cut into a size of 2×2 cm^2 and soaked in ethanol until the CAM was completely removed. Neither heating nor ultrasound was required for this removal, and it only took 6 h. These are the advantages of using CAM compared to using sucrose particles or NaCl particles. Finally, the sample was placed in an oven at 80 °C for 2 h to dry, and a soft and air-permeable porous PDMS doped with FEP powder was obtained, as shown in Figure S2a.

4.2. Fabrication of the FB-TENG Based on the Porous PDMS. Taking the acrylic (2×2 cm^2) as a substrate, a single-electrode mode FB-TENG used an aluminum (Al) electrode (2×2 cm^2) as a working electrode and a porous PDMS ($2 \times 2 \times 0.3$ cm^3) as a friction material. The porous PDMS was attached to the Al electrode by double-sided polyimide tape. A single-sided polyimide tape (Kapton film) or other materials (such as finger, weight, head model) were used as another movable friction material. According to this method, the FB-TENG device based on the porous PDMS was obtained. The detailed production process is displayed in Scheme S1.

4.3. Characterization and Measurement. The SEM morphology and EDS analysis of the porous PDMS were characterized by a Nova NanoSEM 450 and TEAM EDS. The morphology and size of the CAM particles were measured by an upright optical microscope. The FB-TENG was driven by a linear motor (LinMot E1100). The output signals (V_{oc}, I_{sc}, and Q_{sc}) of the FB-TENG were acquainted by a Keithley 6514 electrometer. The output voltage signals of the sensor array were measured by the synchronous data acquisition card (PXIe-4300, National Instruments). The breathability was measured using an air permeability tester (TQD-G1 and VAC-V1).

ASSOCIATED CONTENT

Ⓢ Supporting Information

The Supporting Information is available free of charge at https://pubs.acs.org/doi/10.1021/acsami.2c03056.

> Fabrication process of the FB-TENG; the morphologies and size distributions of three CAM particles; photograph of the porous PDMS sample (2×2 cm^2); ability of a porous PDMS sample (2×3 cm^2) carrying a 1 kg weight; compression and resilience test of the porous

PDMS (made with 74 ± 6 μm CAM particles and 10 wt % FEP powder); SEM image of the porous PDMS (made with 74 ± 6 μm CAM particles and FEP powder content of 10 wt %); EDS image of PDMS with FEP powder 10 wt %; real-time short-circuit current (I_{sc}) signals during one cycle; I_{sc} and the Q_{sc} of the FB-TENG at different frequencies; external current and output power under different load resistances of the FB-TENG (made with 74 ± 6 μm CAM particles and 10 wt % FEP powder); charging curve of different capacitors charged by the FB-TENG (made with 74 ± 6 μm CAM particles and 10 wt % FEP powder); real-time output current and charge of the FB-TENG under different forces; surface SEM images of a solid PDMS and the porous PDMS with CAM particle sizes of 860 ± 70, 290 ± 16 μm; SEM image of PDMS with FEP 0, 5, 15, 20, and 30 wt %; schematic diagram of the fabrication process of the 8 × 8 FB-TENG sensor array; photograph of the 8 × 8 FB-TENG sensor array; schematic diagram of signal collection and processing process based on the 8 × 8 FB-TENG sensor array; schematic diagram of the multichannel signal statistics program; 3D real-time output voltage of a weight, rectangular square, a fist, and an N-letter pattern on the surface of the 8 × 8 FB-TENG sensor array; real-time output voltage when writing N and G with a finger; schematic diagram of the smart pillow monitoring head movement; photograph of the smart pillow; picture with the head pressed in the middle of the smart pillow and the corresponding two-dimensional output voltage intensity map; 3D real-time output voltage of the head model on the surface of the smart pillow; demonstration diagram of the corresponding output signal of the head pressure during turning from the upward to the left or to the right and then back to the upward; and schematic diagram of the head in the most edge position (PDF)

> Light-up LEDs (MP4)

> Simple graphical mapping (MP4)

> Track monitoring writing letters "T, E, N, and G" (MP4)

> Head movement monitoring (MP4)

> Monitoring the danger of falling out of bed (MP4)

■ AUTHOR INFORMATION

Corresponding Authors

Ding Li — *Center on Nanoenergy Research, School of Physical Science and Technology, Guangxi University, Nanning 530004, P. R. China; Beijing Key Laboratory of Micro-Nano Energy and Sensor, Beijing Institute of Nanoenergy and Nanosystems, Chinese Academy of Sciences, Beijing 101400, P. R. China; School of Nanoscience and Technology, University of Chinese Academy of Sciences, Beijing 100049, P. R. China;* ⓞ orcid.org/0000-0001-7286-8907; Email: liding@binn.cas.cn

Zhong Lin Wang — *Beijing Key Laboratory of Micro-Nano Energy and Sensor, Beijing Institute of Nanoenergy and Nanosystems, Chinese Academy of Sciences, Beijing 101400, P. R. China; School of Nanoscience and Technology, University of Chinese Academy of Sciences, Beijing 100049, P. R. China; School of Materials Science and Engineering, Georgia Institute of Technology, Atlanta, Georgia 30332-*

0245, United States; ● orcid.org/0000-0002-5530-0380;
Email: zhong.wang@mse.gatech.edu

Authors

Haiying Kou − Center on Nanoenergy Research, School of Physical Science and Technology, Guangxi University, Nanning 530004, P. R. China; Beijing Key Laboratory of Micro-Nano Energy and Sensor, Beijing Institute of Nanoenergy and Nanosystems, Chinese Academy of Sciences, Beijing 101400, P. R. China; ● orcid.org/0000-0003-1700-8458

Haiming Wang − Beijing Key Laboratory of Micro-Nano Energy and Sensor, Beijing Institute of Nanoenergy and Nanosystems, Chinese Academy of Sciences, Beijing 101400, P. R. China; School of Nanoscience and Technology, University of Chinese Academy of Sciences, Beijing 100049, P. R. China

Renwei Cheng − Beijing Key Laboratory of Micro-Nano Energy and Sensor, Beijing Institute of Nanoenergy and Nanosystems, Chinese Academy of Sciences, Beijing 101400, P. R. China; School of Nanoscience and Technology, University of Chinese Academy of Sciences, Beijing 100049, P. R. China; ● orcid.org/0000-0002-4350-9734

Yanjun Liao − Center on Nanoenergy Research, School of Physical Science and Technology, Guangxi University, Nanning 530004, P. R. China; Beijing Key Laboratory of Micro-Nano Energy and Sensor, Beijing Institute of Nanoenergy and Nanosystems, Chinese Academy of Sciences, Beijing 101400, P. R. China; ● orcid.org/0000-0003-0237-9440

Xue Shi − Beijing Key Laboratory of Micro-Nano Energy and Sensor, Beijing Institute of Nanoenergy and Nanosystems, Chinese Academy of Sciences, Beijing 101400, P. R. China; School of Nanoscience and Technology, University of Chinese Academy of Sciences, Beijing 100049, P. R. China; ● orcid.org/0000-0002-6732-7580

Jianjun Luo − Beijing Key Laboratory of Micro-Nano Energy and Sensor, Beijing Institute of Nanoenergy and Nanosystems, Chinese Academy of Sciences, Beijing 101400, P. R. China; School of Nanoscience and Technology, University of Chinese Academy of Sciences, Beijing 100049, P. R. China

Complete contact information is available at:
https://pubs.acs.org/10.1021/acsami.2c03056

Author Contributions

[⊥]H.K., H.W., and R.C. contributed equally; H.K., D.L., and H.W. conceived the idea under the supervision of Z.L.W; H.K. and H.W. designed and fabricated the structure of FB-TENG and sensor array; H.K., H.W., R.C., Y.L., X.S., D.L., and J.L. performed the measurements and did data analysis; and H.K., D.L., and Z.L.W. discussed the data and prepared the manuscript with input from all authors.

Notes

The authors declare no competing financial interest.

■ REFERENCES

(1) Jin, J. Checking Blood Pressure at Home. *JAMA* **2017**, *318*, 310.

(2) Kim, J.; Chou, E. F.; Le, J.; Wong, S.; Chu, M.; Khine, M. Soft Wearable Pressure Sensors for Beat-to-Beat Blood Pressure Monitoring. *Adv. Healthcare Mater.* **2019**, *8*, No. 1900109.

(3) He, W.; Ye, Y.; Lu, L.; Cheng, Y.; Li, Y.; Wang, Z. Robust Heart Rate Monitoring for Quasi-Periodic Motions by Wrist-Type PPG Signals. *IEEE J. Biomed. Health Inf.* **2020**, *24*, 636−648.

(4) Lin, Z.; Chen, J.; Li, X.; Zhou, Z.; Meng, K.; Wei, W.; Yang, J.; Wang, Z. L. Triboelectric Nanogenerator Enabled Body Sensor Network for Self-Powered Human Heart-Rate Monitoring. *ACS Nano* **2017**, *11*, 8830−8837.

(5) Wang, R.; Mu, L.; Bao, Y.; Lin, H.; Ji, T.; Shi, Y.; Zhu, J.; Wu, W. Holistically Engineered Polymer-Polymer and Polymer-Ion Interactions in Biocompatible Polyvinyl Alcohol Blends for High-Performance Triboelectric Devices in Self-Powered Wearable Cardiovascular Monitorings. *Adv. Mater.* **2020**, *32*, No. 2002878.

(6) Yang, J.; Chen, J.; Su, Y.; Jing, Q.; Li, Z.; Yi, F.; Wen, X.; Wang, Z.; Wang, Z. L. Eardrum-Inspired Active Sensors for Self-Powered Cardiovascular System Characterization and Throat-Attached Anti-Interference Voice Recognition. *Adv. Mater.* **2015**, *27*, 1316−1326.

(7) He, H.; Guo, J.; Illés, B.; Géczy, A.; Istók, B.; Hliva, V.; Török, D.; Kovács, J. G.; Harmati, I.; Molnár, K. Monitoring Multi-Respiratory Indices Via a Smart Nanofibrous Mask Filter Based on a Triboelectric Nanogenerator. *Nano Energy* **2021**, *89*, No. 106418.

(8) Wang, S.; Tai, H.; Liu, B.; Duan, Z.; Yuan, Z.; Pan, H.; Su, Y.; Xie, G.; Du, X.; Jiang, Y. A Facile Respiration-Driven Triboelectric Nanogenerator for Multifunctional Respiratory Monitoring. *Nano Energy* **2019**, *58*, 312−321.

(9) Siegel, J. M. Clues to the Functions of Mammalian Sleep. *Nature* **2005**, *437*, 1264−1271.

(10) Daniela, T.; Couyoumdjian, A.; Curcio, G.; Moroni, F.; Marzano, C.; De Gennaro, L.; Ferrara, M. Lack of Sleep Affects the Evaluation of Emotional Stimuli. *Brain. Res. Bull.* **2010**, *82*, 104−108.

(11) Wagner, U.; Gais, S.; Haider, H.; Verleger, R.; Born, J. Sleep Inspires Insight. *Nature* **2004**, *427*, 352−355.

(12) Stickgold, R. Sleep-Dependent Memory Consolidation. *Nature* **2005**, *437*, 1272−1278.

(13) Grandner, M. A. Sleep, Health, and Society. *Sleep Med. Clin.* **2020**, *15*, 319−340.

(14) Kendzerska, T.; Gershon, A. S.; Hawker, G.; Leung, R. S.; Tomlinson, G. Obstructive Sleep Apnea and Risk of Cardiovascular Events and All-Cause Mortality: A Decade-Long Historical Cohort Study. *PLoS Med.* **2014**, *11*, No. e1001599.

(15) Kushida, C. A.; Littner, M. R.; Morgenthaler, T.; Alessi, C. A.; Bailey, D.; Coleman, J., Jr.; Friedman, L.; Hirshkowitz, M.; Kapen, S.; Kramer, M.; Lee-Chiong, T.; Loube, D. L.; Owens, J.; Pancer, J. P.; Wise, M. Practice Parameters for the Indications for Polysomnography and Related Procedures: An Update for 2005. *Sleep* **2005**, *28*, 499−523.

(16) Boulos, M. I.; Jairam, T.; Kendzerska, T.; Im, J.; Mekhael, A.; Murray, B. J. Normal Polysomnography Parameters in Healthy Adults: A Systematic Review and Meta-Analysis. *Lancet Respir. Med.* **2019**, *7*, 533−543.

(17) Al-Mardini, M.; Aloul, F.; Sagahyroon, A.; Al-Husseini, L. Classifying Obstructive Sleep Apnea Using Smartphones. *J. Biomed. Inf.* **2014**, *52*, 251−259.

(18) Ren, Y.; Wang, C.; Chen, Y.; Yang, J.; Li, H. Noninvasive Fine-Grained Sleep Monitoring Leveraging Smartphones. *IEEE Internet Things J.* **2019**, *6*, 8248−8261.

(19) Camcı, B.; Ersoy, C.; Kaynak, H. Abnormal Respiratory Event Detection in Sleep: A Prescreening System with Smart wearables. *J. Biomed. Inf.* **2019**, *95*, No. 103218.

(20) Chen, Y.; Wang, W.; Guo, Y.; Zhang, H.; Chen, Y.; Xie, L. A Single-Center Validation of the Accuracy of a Photoplethysmography-Based Smartwatch for Screening Obstructive Sleep Apnea. *Nat. Sci. Sleep* **2021**, *13*, 1533−1544.

(21) Fan, F.-R.; Tian, Z.-Q.; Wang, Z. L. Flexible Triboelectric Generator. *Nano Energy* **2012**, *1*, 328−334.

(22) Lin, S.; Xu, L.; Chi Wang, A.; Wang, Z. L. Quantifying Electron-Transfer in Liquid-Solid Contact Electrification and The Formation of Electric Double-Layer. *Nat. Commun.* **2020**, *11*, No. 399.

(23) Wang, Z. L. On Maxwell's Displacement Current for Energy and Sensors: the Origin of Nanogenerators. *Mater. Today* **2017**, *20*, 74−82.

(24) Wang, Z. L. Triboelectric Nanogenerator (TENG)-Sparking an Energy and Sensor Revolution. *Adv. Energy Mater.* **2020**, *10*, No. 2000137.

(25) Zou, H.; Zhang, Y.; Guo, L.; Wang, P.; He, X.; Dai, G.; Zheng, H.; Chen, C.; Wang, A. C.; Xu, C.; Wang, Z. L. Quantifying the Triboelectric Series. *Nat. Commun.* **2019**, *10*, No. 1427.

(26) Wang, Z. L.; Jiang, T.; Xu, L. Toward the Blue Energy Dream by Triboelectric Nanogenerator Networks. *Nano Energy* **2017**, *39*, 9−23.

(27) Zhong, W.; Xu, L.; Yang, X.; Tang, W.; Shao, J.; Chen, B.; Wang, Z. L. Open-Book-Like Triboelectric Nanogenerators Based on Low-Frequency Roll-Swing Oscillators for Wave Energy Harvesting. *Nanoscale* **2019**, *11*, 7199−7208.

(28) Wu, C.; Tetik, H.; Cheng, J.; Ding, W.; Guo, H.; Tao, X.; Zhou, N.; Zi, Y.; Wu, Z.; Wu, H.; Lin, D.; Wang, Z. L. Electrohydrodynamic Jet Printing Driven by a Triboelectric Nanogenerator. *Adv. Funct. Mater.* **2019**, *29*, No. 1901102.

(29) Wang, Z. L. Triboelectric nanogeratorators as New Energy Technology for Self-Powered Systems and as Active mechanical and Chemical Sensor. *ACS Nano* **2013**, *7*, 9533−9557.

(30) Cao, R.; Zhao, S.; Li, C. Free Deformable Nanofibers Enhanced Tribo-Sensors for Sleep and Tremor Monitoring. *ACS Appl. Electron. Mater.* **2019**, *1*, 2301−2307.

(31) Liu, Y.; Zhao, L.; Avila, R.; Yiu, C.; Wong, T.; Chan, Y.; Yao, K.; Li, D.; Zhang, Y.; Li, W.; Xie, Z.; Yu, X. Epidermal Electronics for Respiration Monitoring Via Thermo-Sensitive Measuring. *Mater. Today Phys.* **2020**, *13*, No. 100199.

(32) Song, W.; Gan, B.; Jiang, T.; Zhang, Y.; Yu, A.; Yuan, H.; Chen, N.; Sun, C.; Wang, Z. L. Nanopillar Arrayed Triboelectric Nanogenerator as a Self-Powered Sensitive Sensor for a Sleep Monitoring System. *ACS Nano* **2016**, *10*, 8097−8103.

(33) Yue, O.; Wang, X.; Hou, M.; Zheng, M.; Bai, Z.; Cui, B.; Cha, S.; Liu, X. Skin-Inspired Wearable Self-Powered Electronic Skin with Tunable Sensitivity for Real-Time Monitoring of Sleep Quality. *Nano Energy* **2022**, *91*, No. 106682.

(34) Zhang, H.; Zhang, J.; Hu, Z.; Quan, L.; Shi, L.; Chen, J.; Xuan, W.; Zhang, Z.; Dong, S.; Luo, J. Waist-Wearable Wireless Respiration Sensor Based on Triboelectric Effect. *Nano Energy* **2019**, *59*, 75−83.

(35) Lin, Z.; Yang, J.; Li, X.; Wu, Y.; Wei, W.; Liu, J.; Chen, J.; Yang, J. Large-Scale and Washable Smart Textiles Based on Triboelectric Nanogenerator Arrays for Self-Powered Sleeping Monitoring. *Adv. Funct. Mater.* **2018**, *28*, No. 1704112.

(36) Zhou, Z.; Padgett, S.; Cai, Z.; Conta, G.; Wu, Y.; He, Q.; Zhang, S.; Sun, C.; Liu, J.; Fan, E.; Meng, K.; Lin, Z.; Uy, C.; Yang, J.; Chen, J. Single-Layered Ultra-Soft Washable Smart Textiles for All-Around Ballistocardiograph, Respiration, and Posture Monitoring During Sleep. *Biosens. Bioelectron.* **2020**, *155*, No. 112064.

(37) Fan, Y. J.; Meng, X. S.; Li, H. Y.; Kuang, S. Y.; Zhang, L.; Wu, Y.; Wang, Z. L.; Zhu, G. Stretchable Porous Carbon Nanotube-Elastomer Hybrid Nanocomposite for Harvesting Mechanical Energy. *Adv. Mater.* **2017**, *29*, No. 1603115.
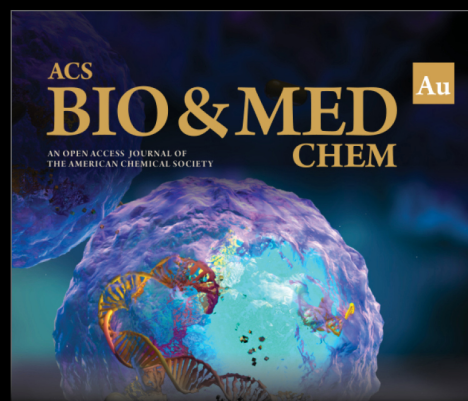
(38) Su, L.; Jiang, Z.; Tian, Z.; Wang, H.; Wang, H.; Zi, Y. Self-Powered, Ultrasensitive, and High-Resolution Visualized Flexible Pressure Sensor Based on Color-Tunable Triboelectrification-Induced Electroluminescence. *Nano Energy* **2021**, *79*, No. 105431.

(39) Yu, C.; Yu, C.; Cui, L.; Song, Z.; Zhao, X.; Ma, Y.; Jiang, L. Facile Preparation of the Porous PDMS Oil-Absorbent for Oil/Water Separation. *Adv. Mater. Interfaces* **2017**, *4*, No. 1600862.

(40) Jiang, Y.; Dong, K.; Li, X.; An, J.; Wu, D.; Peng, X.; Yi, J.; Ning, C.; Cheng, R.; Yu, P.; Wang, Z. L. Stretchable, Washable, and Ultrathin Triboelectric Nanogenerators as Skin-Like Highly Sensitive Self-Powered Haptic Sensors. *Adv. Funct. Mater.* **2020**, *31*, No. 2005584.

(41) Chun, J.; Kim, J. W.; Jung, W.-s.; Kang, C.-Y.; Kim, S.-W.; Wang, Z. L.; Baik, J. M. Mesoporous Pores Impregnated with Au Nanoparticles as Effective Dielectrics for Enhancing Triboelectric Nanogenerator Performance in Harsh Environments. *Energy Environ. Sci.* **2015**, *8*, 3006−3012.